International Journal of Nanomedicine

Dovepress
open access to scientific and medical research

Open Access Full Text Article

ORIGINAL RESEARCH

Regulating Tumor-Associated Macrophage Polarization by Cyclodextrin-Modified PLGA Nanoparticles Loaded with R848 for Treating Colon Cancer

Haohua Yuan[1], Huan Gui[1], Shuanghui Chen[1], Lan Zhu[1], Chenglv Wang[1], Qianyu Jing[2], Hang Lv[1], Quan Wan[2], Shuyi Wang[1], Shengwen Zhou[1], Xiaodong Ren[1], Yingjie Nie[1,3], Linzhao Li[1]

[1]Medical College, Guizhou University, Guizhou Province, 550025, People's Republic of China; [2]School of Preclinical Medicine of Zunyi Medical University, Zunyi, Guizhou Province, 563000, People's Republic of China; [3]NHC Key Laboratory of Pulmonary Immunological Diseases, Guizhou Provincial People's Hospital, Guiyang, Guizhou Province, 550002, People's Republic of China

Correspondence: Yingjie Nie; Linzhao Li, Medical College of Guizhou University, Guiyang, Guizhou Province, 550025, People's Republic of China, Tel +86-085188274013; +86-085188274016, Email nienyj@hotmail.com; lzli@gzu.edu.cn

Purpose: This study aimed to develop a novel and feasible modification strategy to improve the solubility and antitumor activity of resiquimod (R848) by utilizing the supramolecular effect of 2-hydroxypropyl-beta-cyclodextrin (2-HP-β-CD).

Methods: R848-loaded PLGA nanoparticles modified with 2-HP-β-CD (CD@R848@NPs) were synthesized using an enhanced emulsification solvent-evaporation technique. The nanoparticles were then characterized in vitro by several methods, such as scanning electron microscopy (SEM), differential scanning calorimetry (DSC), Fourier transform infrared (FTIR) spectroscopy, particle size analysis, and zeta potential analysis. Then, the nanoparticles were loaded with IR-780 dye and imaged using an in vivo imaging device to evaluate their biodistribution. Additionally, the antitumor efficacy and underlying mechanism of CD@R848@NPs in combination with an anti-TNFR2 antibody were investigated using an MC-38 colon adenocarcinoma model in vivo.

Results: The average size of the CD@R848@NPs was 376 ± 30 nm, and the surface charge was 21 ± 1 mV. Through this design, the targeting ability of 2-HP-β-CD can be leveraged and R848 is delivered to tumor-supporting M2-like macrophages in an efficient and specific manner. Moreover, we used an anti-TNFR2 antibody to reduce the proportion of Tregs. Compared with plain PLGA nanoparticles or R848, CD@R848@NPs increased penetration in tumor tissues, dramatically reprogrammed M1-like macrophages, removed tumors and prolonged patient survival.

Conclusion: The new nanocapsule system is a promising strategy for targeting tumor, reprogramming tumor -associated macrophages, and enhancement immunotherapy.

Keywords: R848, 2-HP-β-CD, anti-TNFR2, TIME, immunotherapy

Introduction

Cancer remains the leading cause of global mortality, and its incidence is projected to increase by 47% by 2040.[1,2] Over the past decade, the development of immunotherapies has revolutionized cancer treatment and garnered attention from clinicians and cancer patients worldwide.[3–5] Cancer immunity is closely linked to the tumor immunosuppressive microenvironment (TIME), which is caused by tumor-associated macrophages (TAMs) and regulatory T cells (Tregs).[6] Notably, M2-like TAMs are prevalent among tumor-infiltrating immune cells, and their abundance often correlates with a poor prognosis.[7] Treatments for TAMs can be divided into the following principal strategies: 1) directly eliminating or depleting TAMs, 2) inhibiting the recruitment of TAMs, and 3) reprogramming tumor-promoting M2 macrophages within TAMs into antitumor M1 macrophages. The first approach may lead to unforeseen side effects, and inhibiting TAM recruitment could reduce therapeutic efficacy due to compensatory proliferation.[8] The third strategy can effectively reduce the number of M2 macrophages,

Received: 8 December 2023
Accepted: 10 April 2024
Published: 17 April 2024

increase the secretion of TNF-α, IL-6, and other cytokines, activate antitumor immune responses, reshape the immunosuppressive tumor microenvironment, and kill tumor cells. Numerous reports have demonstrated that tumors can be effectively treated by drug delivery systems that utilize a 'turn enemies into friends' approach, ushering in a new era of tumor treatment.[9–11] Resiquimod (R848) can polarize TAMs from the M2-like phenotype to the M1-like phenotype.[12–14] However, the pharmacokinetics of R848 are suboptimal, particularly when the drug is administered in the peritoneal cavity; due to its relatively small size, R848 is rapidly diffused and leads to subsequent systemic toxicity.[15–17] Conversely, the effectiveness of TLR7/8 agonists in cancer treatment may be improved by employing drug delivery strategies that enhance drug retention and targeted delivery while minimizing off-target toxicity.[17,18]

Several nanomaterial-based immunomodulatory treatments can effectively target immunomodulatory agents, enhance immune responses at reduced doses, and lower systemic toxicity.[19] Poly(D,L-lactic-co-glycolic acid) (PLGA), an FDA-approved biodegradable polymer, stands out for its biocompatibility, safety, and controllable biodegradation rate.[3,20] Another seven-unit cyclic oligosaccharide compound, 2-hydroxypropyl-β-cyclodextrin (2-HP-β-CD), can notably increase water solubility when hydroxypropyl is incorporated.[21] Moreover, 2-HP-β-CD has a natural affinity to macrophages.[22] This compound naturally gravitates toward macrophages and can effectively solubilize numerous drugs that are usually insoluble in water. Recently, researchers have investigated the ability of R848-loaded cyclodextrin nanoparticles to enhance TAM targeting in vivo.[23] Furthermore, tumor necrosis factor receptor type II (TNFR2) is the primary receptor of TNF in murine and human Treg cells.[24,25] Accordingly, targeting TNFR2 can suppress Treg activity.

To address the limitations of TLR agonists, particularly their systemic toxic side effects in clinical settings, we developed a novel approach using PLGA nanocarriers to encapsulate the drug R848, denoted R848@NPs. Additionally, we used 2-HP-β-CD, denoted CD@R848@NPs, to modify the PLGA carrier; this modification improved drug solubility and macrophage polarization while safeguarding the nanoparticles from aggregation and phagocytosis within the body (Figure 1a). To investigate nanoparticle localization in vivo, we utilized in vivo imaging by incorporating the fluorescent dye IR-780 (IR-780-R848@NPs) (a control group) or IR-780-CD@R848@NPs. The morphology and state of the nanoparticles were investigated using transmission electron microscopy (TEM), Fourier transform infrared spectroscopy (FTIR), and differential scanning calorimetry (DSC) techniques.[22] Comprehensive in vitro and in vivo evaluations were conducted to determine the therapeutic potential of combining CD@R848@NPs with anti-TNFR2 (A-T) in a cancer

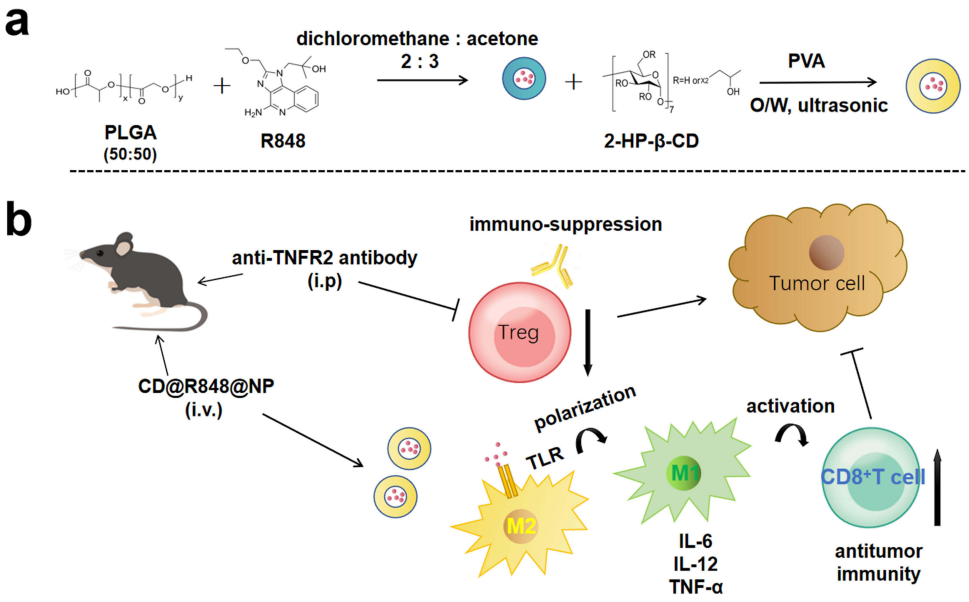

Figure 1 Schematic diagram of mechanism of this research: (a) Illustration of the synthesis of CD@R848@NPs; (b) CD@R848@NPs combined with anti-TNFR2 (CD@R848@NPs+A-T) therapy, aimed at selectively reprogramming M2-like to M1-like macrophages in TIME and provide further activation signals to $CD8^+$ T lymphocytes potentiating antitumor immunity by increased secretion of proinflammatory cytokines (such as IL-6, IL-12 and TNF-α). On the other hand, anti-TNFR2 can inhibit immune tolerance by decrease Tregs function. The nanoparticles increase the delivery of R848, thus, enhancing the therapeutic effect.
Notes: anti-TNFR2: A-T, CD@R848@NPs, drug R848-loaded PLGA nanoparticles modified by 2-HP-β-CD.

model (Figure 1b). This approach might offer a straightforward and universally applicable strategy for delivering other hydrophobic cancer drugs on demand.

Materials and Methods

Chemicals

Resiquimod (R848) was purchased from Selleck (Houston, TX, USA). Poly(D, L-lactic-co-glycolic acid) (PLGA) (LA: GA = 50:50, 10–20 kDa) and cell counting kit-8 (CCK-8) were purchased from MedChenExpress (Monmouth Junction, NJ, USA). Poly(vinyl alcohol) (PVA), the heptamethine indocyanine dye IR-780 iodide, and 2-hydroxypropyl-β-cyclodextrin (2-HP-β-CD) were obtained from Sigma-Aldrich Co. (St Louis, MO, USA). The anti-mouse TNFR2 (CD120b) antibody was purchased from Bio X Cell (West Lebanon, NH). Hoechst 33,342 and LysoTracker Red DND-99 were purchased from Yeasen Biotechnology (Shanghai, China). All other reagents used were of the highest commercially available grade.

Animals

If not otherwise indicated, animal experiments were performed using C57BL/6 mice (SPF) acquired from Spaefer Biotechnology Co, Ltd. (Beijing, China). Breeding conditions are as follows: regular lighting, temperature of 20–25°C, constant humidity, air filtration, and free food and drinking water. Protocols for animal study were approved by the Institutional Animal Care and Use Committee (IACUC) of Guizhou University.

Cells

Cell cultures were conducted in the specified medium at a temperature of 37°C, in the presence of 5% CO_2. Regular monitoring was conducted to ensure absence of mycoplasma contamination. RAW 264.7 cells, utilized in investigations pertaining to the uptake of nanoparticles, were acquired from ATCC and underwent cultivation in Dulbecco's Modified Eagles Medium (abbreviated as DMEM; manufactured by GIBCO). These cells were initially seeded at a concentration of 1×10^6 cells/mL, with 6-well plates serving as the experimental setup for qPCR analysis, while 12-well plates were utilized for image analysis. Subsequently, treatment involving the administration of 20 ng/mL of recombinant mouse IL-4 (courtesy of PeproTech) was carried out over a period of 48 hours in order to elicit an M2-like phenotype.

Preparation of Different Nanoparticles

R848-loaded nanoparticles (R848@NPs) were synthesized by employing the oil-in-water single-emulsion method as previously described.[26] The aqueous phase for this synthesis comprised a 1% w/v polyvinyl alcohol (PVA) solution. In the organic phase, 40 mg of poly(D,L-lactic-co-glycolic acid) (PLGA) and 2 mg of R848 were dissolved in 1.0 mL of acetone/dichloromethane (3:2). The resultant mixture was sonicated for 10 minutes to create an emulsion. This organic solution was gradually introduced into 20 mL of the aqueous PVA solution under ultrasonication (Kunshan Ultrasonic Instrument Co., Shanghai, China).) in an ice bath for 20 minutes, employing 3-second on and 3-second off pulses, resulting in the formation of an oil-in-water (O/W) emulsion. Unloaded nanoparticle cores (CD@NPs) were fabricated using the same procedure without R848 in the organic phase.

To synthesize CD@R848@NPs, a solution containing a mixture of 2-HP-β-CD (0.5% w/v in 1% PVA in distilled water) was utilized as the dispersing phase during the emulsion solvent diffusion process. The subsequent steps were identical to those used to prepare R848@NPs. Nanoparticles were collected and washed through three centrifugation cycles at 13,000 rpm for 10 minutes each. Fluorescent dye-labeled nanoparticles (IR-780-CD@R848@NPs) were synthesized by substituting R848 with 2 mg of IR-780 dye, and all other conditions remained unchanged. The method of preparing IR-780-R848@NPs was similar to that mentioned above, except that 2-HP-β-CD was not present in the aqueous phase.

Characterization of Different NP Formulations

A Malvern Laser Particle Size Analyzer (Nano ZS90, Malvern Instruments Ltd., UK) was used to comprehensively analyze the nanoparticle characteristics, including their particle size, zeta potential, and polydispersity index (PDI). Prior to the measurements, all the samples were resuspended in deionized water (ddH2O) at a concentration of 1 mg/mL and subjected to 20 minutes of sonication.[27,28] To examine the nanoparticle morphology, a JEM-2100 instrument (JEOL Ltd., Japan) was utilized for transmission electron microscopy (TEM) analysis.

Loading Capacity and Entrapment Efficiency

To isolate the nanoparticles from any residual drug, the sample solution was washed repeatedly with water and centrifuged at 1000 rpm for 10 minutes. The supernatant was then transferred to a 3-KD ultrafiltration tube and subjected to a second centrifugation at 4 °C for 30 minutes at 9000 rpm to separate the nanoparticles from any small amount of the dissolved drug. The amount of R848 released was measured using UV–vis spectroscopy. The following equations were used to calculate the loading capacity (LC) and entrapment efficiency (EE):

$$EE(\%)=\frac{W1-W2}{W0}\times 100\%$$

$$LC(\%)=\frac{W1-W2}{W3}\times 100\%$$

The passage provides information about the following variables: W_0, W_1, W_2, and W_3. W_0 represents the total amount of R848, W_1 represents the amount of R848 in the supernatant after low-speed centrifugation, W_2 represents the amount of R848 in the 3-KD ultrafiltration filtrate, and W_3 represents the weight of the nanoparticles.

Fourier Transform Infrared Spectroscopy (FTIR)

For the analysis of R848 and the modified nanoparticle compositions, infrared spectroscopy experiments were conducted with an FTIR spectrometer (Nicolet 5 FTIR, Thermo Scientific, Waltham, MA, USA). The objective was to identify distinctive functional groups and elucidate the fabrication process of the nanoparticle system. To achieve this goal, the samples were blended with KBr powder, compacted into discs, and subsequently analyzed across a wavenumber range of 4000–400 cm^{-1}.

Differential Scanning Calorimetry (DSC)

The sample was heated in a controlled manner by utilizing a sealed aluminum pan with a heating rate of 5 mL/min. DSC thermograms were generated using an automatic thermal analyzer (TA-20, Shimadzu, Tokyo, Japan) with a temperature range of 30–300 °C. Notably, each sample contained a consistent quantity of 5 mg.

In vitro Release Profiles

To investigate the pH-dependent drug release kinetics, 20 mg of nanoparticles were dispersed in either 60 mL of release medium (PBS+0.1% w/v Tween 80) with a pH of 7.4 or an environment simulating late endosomes/lysosomes with a pH of 5.0.[29,30] The dispersion process was performed at 37 °C using a dialysis tube with a molecular weight cutoff of 3.5 kDa. At specific time intervals, precisely 1 mL of the dialysate was sampled to measure the absorbance of R848 at a wavelength of 254 nm. Subsequently, an equivalent volume of fresh PBS was reintroduced into the system to maintain the overall volume. The amount of released R848 was determined using UV–visible spectroscopy.

In vitro Cytotoxicity

To investigate the potential adverse effects of nanoparticles on MC38 cells, MC38 cells were cultured in RPMI 1640 medium supplemented with 10% fetal calf serum. A total of fifty thousand cells were then added to each well of 96-well plates. Next, the cells were exposed to the CD@NPs and CD@R848@NPs, and the concentration of R848 was varied between 5 and 80 μg/mL. After treatment, 10 μL of CCK-8 reagent (MedChem Express, Monmouth Junction, NJ, USA)

was added to each well, and the cells were incubated for 1 hour. Subsequently, the optical densities of the cells were determined at a wavelength of 450 nm using an iMark Microplate Absorbance Reader (Bio-Rad, USA).

In vitro Cellular Uptake Study

To investigate the affinity of the modified nanoparticles for macrophages, we used IR-780 dye as a fluorescent label and loaded it into the nanoparticles. RAW264.7 cells were polarized into M2 macrophages using IL-4 (10 ng/mL) for 24 h[23]. Subsequently, the cells were incubated with different IR-780-loaded nanoparticles (IR-780-R848@NPs and IR-780-CD@R848@NPs) for 6 hours. Following incubation, the cells were washed three times with PBS to prevent further uptake. Then, the cells were fixed with LysoTracker Red DND-99 (Yeasen, Shanghai, China). After 15 minutes, the cells were washed three times with PBS again, and the nuclei were stained with Hoechst for 10 minutes. The internalization process of the modified nanoparticles was observed using a fluorescence inverted microscope.

In vitro Macrophage Repolarization Assay

A total of 1×10^5 RAW 264.7 cells were seeded into each well of a six-well plate, and M2 macrophages were polarized in the same manner as previously described. The cells were then incubated with the nanoparticles at 37 °C for 24 hours, with a final concentration of 1 mg/mL for each nanoparticle. Afterward, both cells and cell supernatants were collected. The cells were stained with the markers CD11b, F4/80, $CD86^+$, and $CD206^+$, and the content was detected using flow cytometry (CytoFlex, Beckman Coulter, USA). To analyze the expression of M1-related genes, RNA was extracted from the harvested cells. Total RNA (2 μg) was reverse transcribed into complementary DNA using HiScriptIII RT SuperMix for qPCR (Vazyme, Shanghai, China). The specific primers used in this process are shown in Supplementary Table 1. The annealing temperatures were further analyzed using Bio-Rad CFX Maestro software.

In vivo Tumor Targeting and Biodistribution

To further investigate the distribution of nanoparticles in mice and the affinity of nanoparticles for tumors, we incorporated the fluorescent dye IR-780 to track and locate the nanoparticles. Subsequently, we subcutaneously injected MC38 cells into BALB/c mice to establish a tumor model. Subsequently, BALB/c mice were intravenously injected with free IR-780 or IR-780-loaded nanoparticles (either IR-780-R848@NP or IR-780-CD@R848@NP) at a dose of 100 μg/kg. Fluorescence images were captured at various time points postinjection using the Lumi III system (USA). Moreover, the biological distribution of IR-780-CD@R848@NPs was analyzed at different intervals post intravenous administration using the same system. Analysis of the fluorescence images was carried out using Living Imaging software.

In vivo Antitumor Efficacy

To further evaluate the antitumor effects of the nanoparticles in vivo, we conducted an experiment using female C57BL/6 mice. On Day 0, we injected 1×10^6 MC38 cells into the right thigh of each mouse to establish a tumor model. The mice were categorized into the following groups: a control group that received PBS, a CD@NP group, an anti-TNFR2 group (A-T), a CD@R848@NP+anti-TNFR2 group (CD@R848@NP+A-T), and an R848+anti-TNFR2 group (R848+A-T). All groups received the same R848 dose (1 mg/kg) via intravenous administration.

Treatment commenced when the tumor volume reached 200–300 mm^3. On Days 12, 16, and 20 after tumor inoculation, control (PBS), R848, CD@R848@NPs, or CD@NPs were intravenously administered to the mice. On Days 13 and 18, the tumor-bearing mice were intraperitoneally injected with anti-TNFR2 (5 mg/kg) or PBS. Tumor growth was monitored with a caliper every two days, and tumor volume was calculated as (length × width × height)/2. After 18 days of treatment, one mouse from each group was randomly selected for imaging. Subsequently, the mice were euthanized, and their tissues (heart, liver, spleen, lungs, kidneys, and tumors) were surgically removed and preserved in formalin solution. The following day, the tissue samples were embedded in paraffin and sliced into thin sections measuring 4~5 μm. These sections were then stained with hematoxylin/eosin (H&E) and mounted on poly-L-lysine-coated glass slides (Safeline Histopathology, Centre, Pune, India). The method of H&E staining is detailed described in the Supplementary file (Material and methods).

Analysis of Antitumor Immunity Activation in vivo

After the full treatment was complete, the mice were sacrificed on 10 days after the last dose (Day 30), and the tumors and spleens were collected. Whole blood was collected and centrifuged at room temperature for 10 minutes at 3500 rpm. The levels of the cytokines IL-12, IL-6, and TNF-α in the serum were detected using ELISA following the instructions provided by the reagent manufacturer. Additionally, flow cytometry was utilized to detect the polarization of macrophages in the tumor group. The cells were washed in FACS buffer and stained with BV510-conjugated anti-mouse CD45 (1:500, BioLegend, clone 30-F11, USA), FITC-conjugated anti-mouse CD11b (1:500, Invitrogen, clone M1/70, USA), F4/80-conjugated anti-mouse PE (1:250, BD/Pharmingen, clone BM8, USA), and CD86-conjugated anti-mouse BV421 (1:500, BD/Pharmingen, clone GL1, USA) for 30 min at 4 °C. The stained cells were examined through a flow cytometer (BD FACSCelesta). Moreover, the infiltration of lymphocyte cells from the spleen and blood was assessed by FCM. The cells were stained with BV510-conjugated anti-mouse CD45 (1:100, BioLegend, clone 30-F11, USA), BV605-conjugated anti-mouse CD3 (1:100, BD/Horizon, clone 145–2C11, USA), and FITC-conjugated anti-mouse CD4 (1:250, BioLegend, clone GK1.5, USA) antibodies. BV421-conjugated anti-mouse CD8 (1:250, BD/Pharmingen, clone 53e6.7, USA) was used.

Tumor tissue from C57BL/6 mice was cryosectioned at a thickness of 8 μm. The frozen sections were stained with primary antibodies for 60 minutes at room temperature and then incubated with secondary antibodies for 30 minutes. Afterward, the sections were counterstained with 4′,6-diamino-2-phenylindole (DAPI). Images were acquired using a confocal microscope (Nikon). The F4/80 (G1231) and CD206 (G1223) antibodies were obtained from Servicebio Technology Co., Ltd. (Wuhan, China).

The secretion of the cytokines IL-6 and TNF-α in mouse tumor tissue sites was assessed through immunohistochemistry (IHC) and histopathology. Goat anti-rabbit TNF-α IgG (1:500; Sigma, USA) and IL-6 (1:500; Sigma, USA) were used for the evaluation.

Rechallenge Experiments in Tumor-Free Mice

To assess the potential immune memory generated by immune combination therapy with nanoparticles in mice, tumor-free mice in the CD@R848@NP+anti-TNFR2 group (CD@R848@NP+A-T) were monitored for 60 days after the last dose (Day 80). On day 61, MC38 tumor cells were subcutaneously inoculated into the right thigh, while an equivalent amount of Hepa1-6 tumor cells was inoculated on the opposite side (left side). Tumor size was systematically observed and recorded every two days.

Statistical Analysis.

If not explicitly stated, all data were reported as the mean ± standard deviation (SD). The mean differences were computed using a two-tailed Student's *t*-test or one-way ANOVA, if deemed suitable, with the use of GraphPad Prism 8. The threshold for statistical significance was established at a significance level of $P < 0.05$.

Results

Characterization of CD@R848@NPs

The TEM images depicted in Figure 2a illustrate the morphologies of various nanoparticles. At magnifications of ×10,000 and ×30,000, individual dispersions of nanoparticles without adhesion were observed. Remarkably, nanoparticles modified with 2-HP-β-CD exhibited a distinct core-shell structure, accompanied by a substantial increase in particle size.

As illustrated in Figure 2b, the CD@R848@NPs and CD@NPs existed in an emulsified state. Over time, the CD@R848@NPs remained stable in PBS at 4 °C. The zeta potential of the nanoparticle suspension was measured, revealing an approximate value of 21 ± 1 mV (Figure 2c). The synthesized CD@R848@NPs was 376 ± 30 nm in size (Figure 2d), and the particle size distribution exhibited a relatively homogeneous pattern. The PDI of the nanoparticle solution was less than 0.2 for all of the samples.

FTIR was employed to determine the successful encapsulation of the drug and analyze the binding mode of R848 and the nanocarriers (Figure 2e). The distinctive peaks observed at 1450 and 1646.4 cm^{-1} in the R848 spectrum correspond to the benzene ring and amide carbonyl, respectively. The spectral range of 2-HP-β-CD, from 3600 to 3200 cm^{-1}, primarily

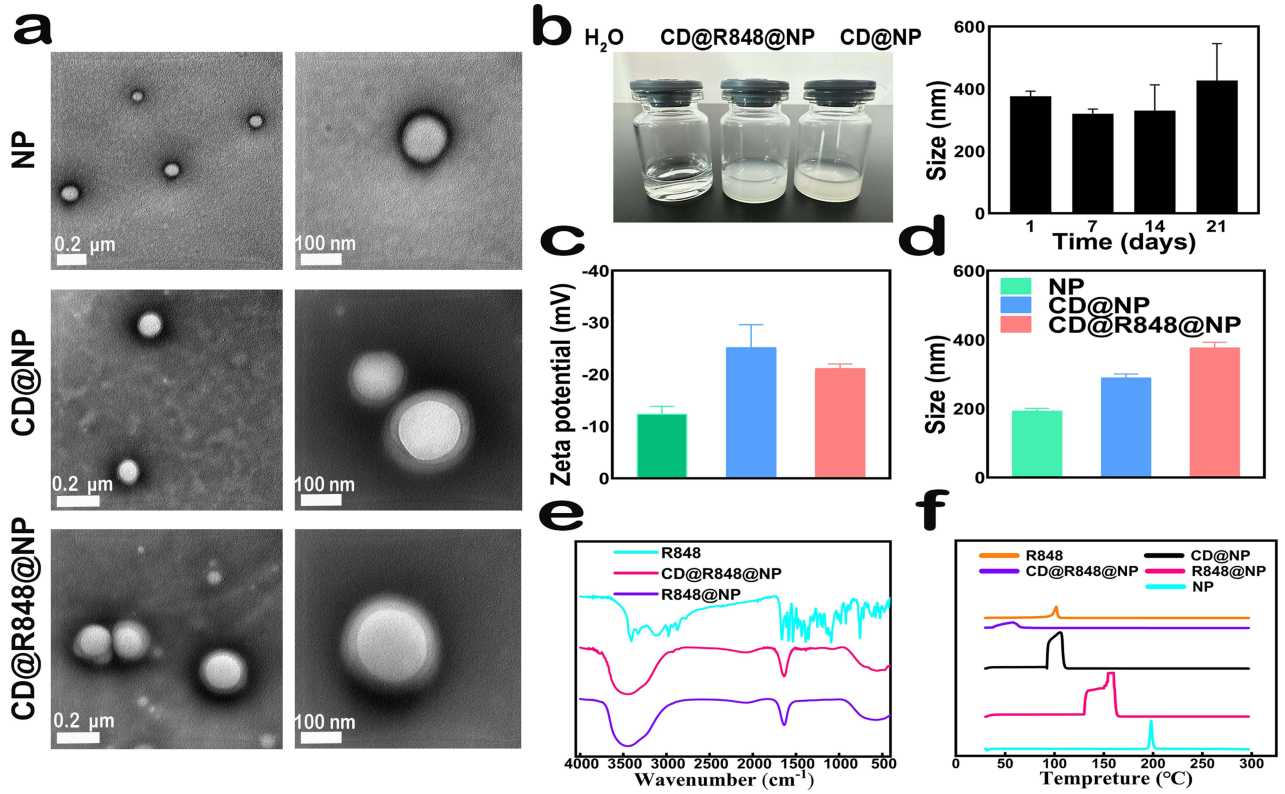

Figure 2 Characterization of CD@R848@NPs and other nanoparticles: (**a**) TEM images showing the morphology of NPs, CD@NPs, and CD@R848@NPs negatively stained with phosphotungstic acid (2% [wt/vol]). (**b**) Morphology of the three groups and micromorphology size stability of CD@R848@NPs over time in PBS buffer. n = 3. (**c-d**) ζ-potential and hydrodynamic diameters of the NPs, CD@NPs, and CD@R848@NPs evaluated by DLS. (**e**) FTIR spectra of R848, R848@NPs, and CD@R848@NPs. n = 3. (**f**) DSC spectra of R848, R848@NPs, and CD@R848@NPs. n = 3.

Notes: NPs, bare PLGA nanoparticles; CD@NPs, PLGA nanocapsules modified with 2-HP-β-CD; R848@NPs, R848 coated with PLGA nanoparticles; CD@R848@NPs, R848-loaded PLGA nanoparticles modified with 2-HP-β-CD.

reflects the stretching vibration of the hydroxyl stretching vibrations. Notably, the characteristic peak of R848 in the CD@R848@NP and CD@NP spectra decreased, whereas the absorption peak resulting from the stretching vibration of amino and hydroxyl groups at 3409 cm^{-1} shifted to 3455 cm^{-1}. This shift suggested that R848 binds to nanoparticles through hydrogen bonds and assumes an amorphous form. Furthermore, the presence of 2-HP-β-CD in the PLGA nanoparticles did not alter the presence of R848. In the spectra of the CD@NPs and CD@R848@NPs, the characteristic absorption peak of R848 vanished, indicating that R848 was successfully encapsulated by the nanoparticles and that the unloaded drugs was removed through centrifugation.

The melting peak of R848 was at approximately 193 °C (Figure 2f). However, for CD@R848@NPs, this melting peak was not observed; instead, a broad peak was observed, indicating that the crystallization process is relatively slow. This observation further confirmed that R848 was successfully encapsulated by the nanoparticles.

The absorbance was measured using ultraviolet–visible (UV–Vis) spectroscopy and plotted on a standard curve. Based on the formula and standard curve of R848 (Supplementary Figure 1), the encapsulation efficiency and drug capacity of R848 in CD@R848@NPs were determined to be 65.36 ± 3% and 3.11 ± 0.61%, respectively.

The release of R848 from CD@R848@NPs was studied by simulating an in vivo environment (Figure 3a). After 72 h of incubation in PBS (pH 7.0) containing 0.1% w/v Tween 80 at 37 °C, 58.85±0.67% of the R848 was released from the nanocapsules. In an esterase-rich environment, 70.16±1.19% of the R848 was released after 72 h. The rate of R848 release increased accordingly with decreasing pH, possibly because the amide bond between PLGA and the carboxyl group of R848 becomes more unstable in acidic solution.[31]

To assess biocompatibility, the cytotoxicity of CD@NPs, R848@NPs, and CD@R848@NPs to MC38 cells was evaluated using a CCK8 assay (Figure 3b). All the nanocapsules exhibited minimal cytotoxicity, indicating their potential

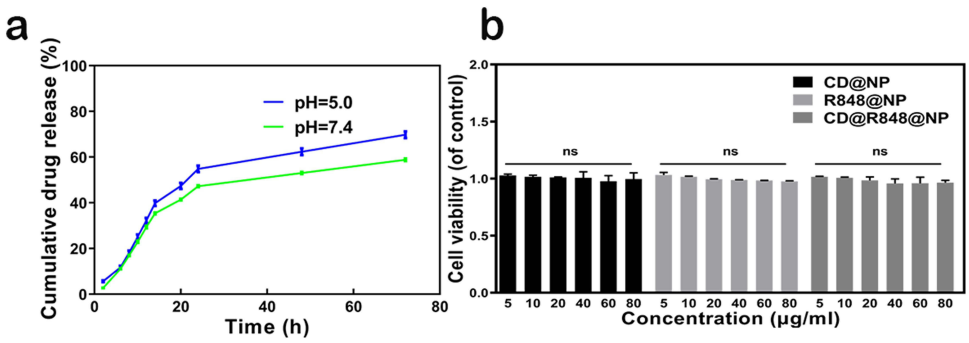

Figure 3 In vitro release profiles and cytotoxicity. (**a**) Cumulative R848 release from CD@R848@NPs in different physiological environments. The data are shown as the means ± SD of three independent experiments. (**b**) The cytotoxicity of CD@NPs, R848@NPs and CD@R848@NPs. Data are displayed as the mean ± SD of three independent experiments and were analyzed with two-way ANOVA followed by Tukey's multiple comparisons test. NS indicate no statistical difference.

as biocompatible nanomaterials and suitable drug delivery carriers. Moreover, the nanocapsules maintained excellent cytocompatibility, even at high concentrations.

An in vitro analysis of hemolysis characteristics (Supplementary Figure 2) revealed no red blood cell lysis in the supernatants of the CD@NP and CD@R848@NP groups when the R848 concentration was between 25 and 100 μg/mL. The method of Hemolysis test is detailed described in the Supplementary file (Material and methods).

CD@R848@NPs Increased Cellular Uptake in vitro

As depicted in Figure 4, the cellular uptake levels of the 2-HP-β-CD-modified nanoparticles were greater than those of the regular nanoparticles, possibly due to the natural affinity of 2-HP-β-CD for macrophages. The fluorescence signals

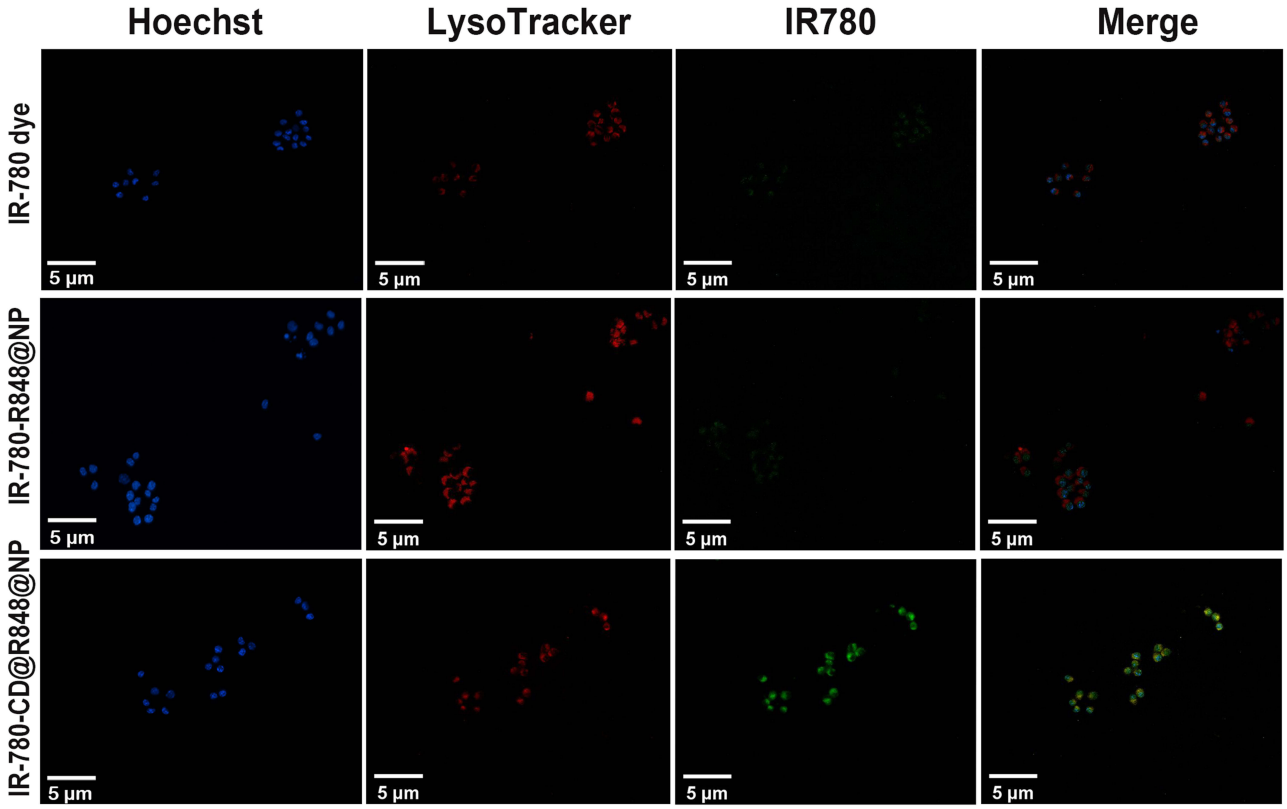

Figure 4 In vitro cellular uptake study: Cellular uptake of IR-780, IR-780-R848@NPs, IR-780-CD@R848@NPs, and RAW264.7 cells (stimulated with the M2-type macrophage activator IL-4 for 24 h before further treatment) for 6 h. CD@R848@NPs were labeled with LysoTracker Red DND-99 (red fluorescence) and IR-780 dye (green fluorescence). Nuclei (blue fluorescence) were stained with Hoechst 33,342. Scale bar = 5 μM.
Notes: IR-780-R848@NPs indicate the drugs R848 and IR-780 dye loaded with PLGA nanoparticles; IR-780-CD@R848@NPs indicate the drugs R848 and IR-780 dye loaded with PLGA nanoparticles modified with 2-HP-β-CD.

from the red and green channels clearly overlap, indicating that the internalized NPs were transported through the lysosomal pathway upon cellular entry. Lysosome-mediated endocytosis is a crucial mechanism for the entry of nanomaterials into cells. Lysosomes are equipped with varying quantities of hydrolases, thereby facilitating the rapid destruction and degradation of internalized NPs, which aligns with the findings of the in vitro release results.

CD@R848@NP Induced Macrophage Reprogramming in vitro

The effect of the nanoparticles on M2-like macrophage repolarization was investigated in vitro. Compared with free R848, R848@NPs and CD@R848@NPs significantly increased the number of M1 macrophages ($F4/80^+$ and $CD86^+$), suggesting that the M2 phenotype was successfully polarized toward the M1 phenotype (Figure 5a–b). No significant differences were observed between R848@NP and CD@R848@NP, which suggested that both the nanomaterials promoted M1 macrophage polarization in vitro.

To further investigate the polarization of macrophages by CD@R848@NPs, we conducted quantitative real-time PCR (qPCR) to analyzed related genes (Figure 5c). The results showed that CD@R848@NPs significantly increased the expression of CD80, TNF-α and nos2 compared to M2 macrophages. Meanwhile, M2-type macrophage markers Mrc1 and Arg1 displayed the opposite tendency in CD@R848@NPs group, which could be attributed to the enhanced polarization of macrophages induced by R848, and 2-HP-β-CD could boost the effect. As showcased in Figure 5c, R848 or R848@NP similarly reduced Mrc1 and Arg1 expression, but the CD80 expression levels were decreased compared with CD@R848@NPs.

Evaluation of the Biological Distribution of CD@R848@NPs in vivo

To evaluate the biodistribution patterns and therapeutic effectiveness of the nanodrugs in vivo, we constructed a hypodermic mouse model of MC38 cancer. The nanoparticles (CD@R848@NPs or R848@NPs) were loaded with a fluorescent dye (IR-780 dye) for biodistribution studies. The mice were intravenously administered the following formulations: IR-780 dye, nanocapsules loaded with IR-780 dye (IR-780-R848@NPs), and 2-HP-β-CD-modified nanocapsules containing IR-780 dye (IR-780-CD@R848@NPs). Each mouse was administered 100 μg/kg of IR-780 dye.

As illustrated in Figure 6a, free IR-780 treatment caused little tumor retention, and fluorescence diminished after 24 h. Both types of nanoparticles labeled with fluorescence were disseminated rapidly throughout the mice, indicating that the nanocapsules exhibited passive biodistribution characteristics. Moreover, while the fluorescence intensity of IR-780-R848@NPs decreased at 24h postinjection, that of IR-780-CD@R848@NPs remained relatively elevated, and the fluorescence signal peaked at 48 h and then weakened slowly. This prolonged circulation effect exhibited by the modified

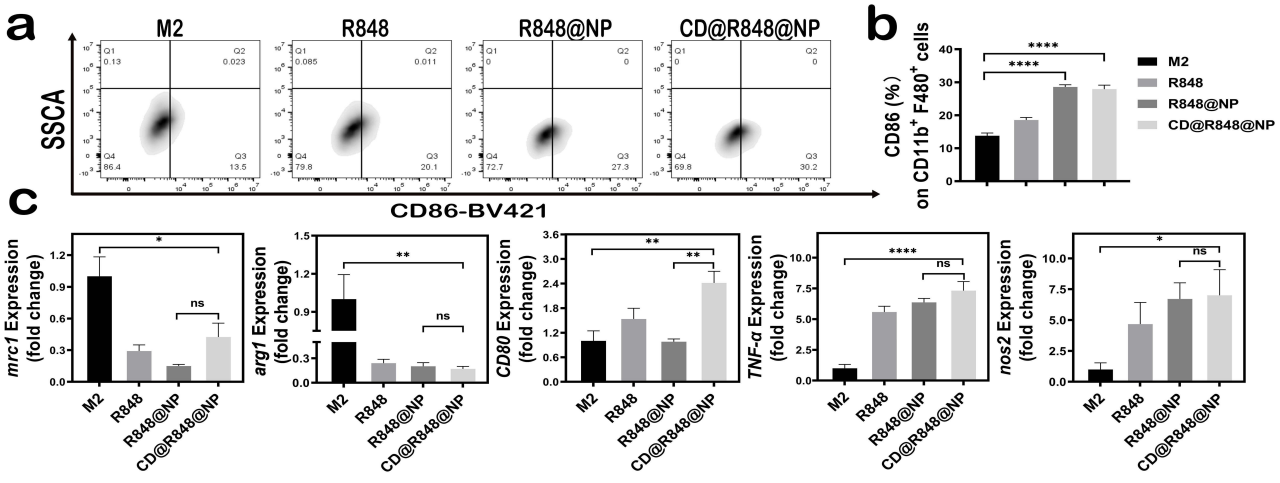

Figure 5 In vitro macrophage reprogramming assay: (**a**) Representative dot plots showing M1-like macrophage repolarization. (**b**) The percentage of M1-like macrophages ($CD86^+$) among $CD11b^+$ $F4/80^+$ cells was analyzed. (**c**) Mrc1, Arg1, CD80, Nos2, and TNF-α gene expression was measured by qPCR. n = 3. All data are expressed as mean ± SEM and was analyzed with one-way ANOVA followed by Sidak's multiple comparisons test. *, p<0.05, **, p<0.01, ****, p<0.0001. NS indicate no statistical difference.

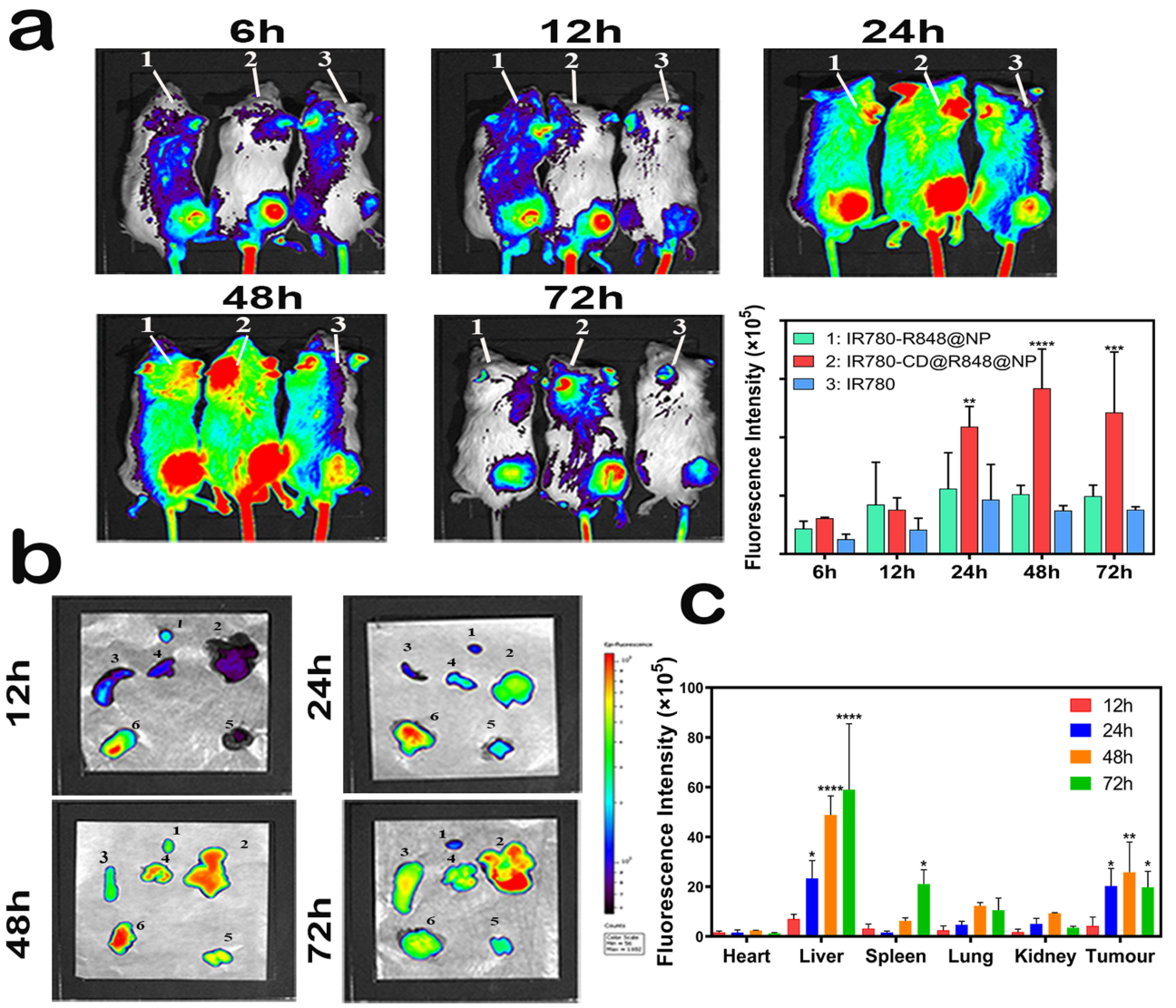

Figure 6 Evaluation of the biological distribution of CD@R848@NPs in vivo: (**a**) In vivo tumor targeting and biodistribution of IR-780, IR-780-R848@NPs, and IR-780-CD @R848@NPs. IR-780 equivalent dose, 100 μg/kg. The fluorescence signals at different time points at the tumor site were analyzed. n = 6. The data are expressed as mean ± SEM and was analyzed with two-way ANOVA followed by Tukey's multiple comparisons test. **, p<0.01, ***, p<0.001, ****, p<0.0001 compared with IR-780. (**b**) Fluorescence images of organs (1: heart; 2: liver; 3: spleen; 4: lungs; 5: kidneys) and tumors (6) at 12, 24, 48 and 72 h. (c) Semiquantitative analysis of tumor fluorescence signals was conducted at different time points using three mice per group (n = 6). The experiment was conducted three times. The data are expressed as mean ± SEM and was analyzed with two-way ANOVA followed by Tukey's multiple comparisons test. *, p<0.05, **, p<0.01, ***, p<0.001, ****, p<0.0001 compared with 12h.

nanoparticles was attributed to the presence of 2-HP-β-CD on the PLGA surface. The abundant hydroxyl groups on the 2-HP-β-CD surface augment the hydrophilicity of PLGA, bolstering its recognition by RES. Consequently, the drug circulation time is prolonged and drug accumulation at cancerous sites is enhanced.[22,32]

Ex vivo imaging of IR-780 fluorescence in the tumor and five important organs was performed when the IR-780-CD @R848@NP group mice were sacrificed at different times (Figure 6b), and quantitative analysis of the results was performed (Figure 6c). Initially, during the early drug metabolism phase, fluorescence signals were localized predominantly in the liver and lungs before concentrating at the tumor site. Among the six organs analyzed, the liver and tumor were the major sites at which all particles accumulated. Remarkably, the tumor showed a bright fluorescence signal at 48 h, consistent with the in vivo biodistribution results. At 72 h postinjection, a notable concentration of nanoparticles was observed in the liver, likely attributable to their uptake by the reticuloendothelial system (RES) and subsequent passive liver targeting.

CD@R848@NPs Exhibit Antitumor Effects on Mice with Colon Cancer

Following the series of in vitro screening experiments as above, CD@R848@NP group exhibited better efficacy in tumor targeting and biodistribution compared with R848@NP group, so the CD@R848@NP was selected for the follow-up in vivo experiment to explore the antitumor efficacy. To evaluate the effect of CD@R848@NPs on macrophage polarization and the tumor microenvironment in vivo, we subcutaneously implanted MC38 cancer cells into female C57BL/6 mice. The experimental design is illustrated in Figure 7a. The treatment groups were PBS (n = 6), CD@NPs (n = 6), anti-TNFR2 (A-T) (n = 6), CD@R848@NPs+anti-TNFR2 (CD@R848@NPs+A-T) (n = 6), and R848+anti-TNFR2 (R848+A-T) (n = 6). Representative images of mice from each group were captured on day 18 after the last dose. Representative images of mice from each group showed that tumors were eliminated in the CD@R848@NPs+A-T group and were significantly reduced in the R848+A-T group compared with PBS group (Figure 7b). Tumor volume analysis revealed no significant differences in tumor growth between the PBS and CD@NP groups. However, significant inhibition of tumor growth was observed in the R848+A-T group. Notably, tumors in the R848+A-T group started to relapse at a later stage, possibly due to immune tolerance or systemic side effects of the drug. This result indicates that the nanodelivery system helps prevent systemic adverse reactions to the drug (Figure 7c). Additionally, the body weights of mice did not change obviously, and survival in the CD@R848@NPs+A-T was significantly extended (Figure 7d and e).

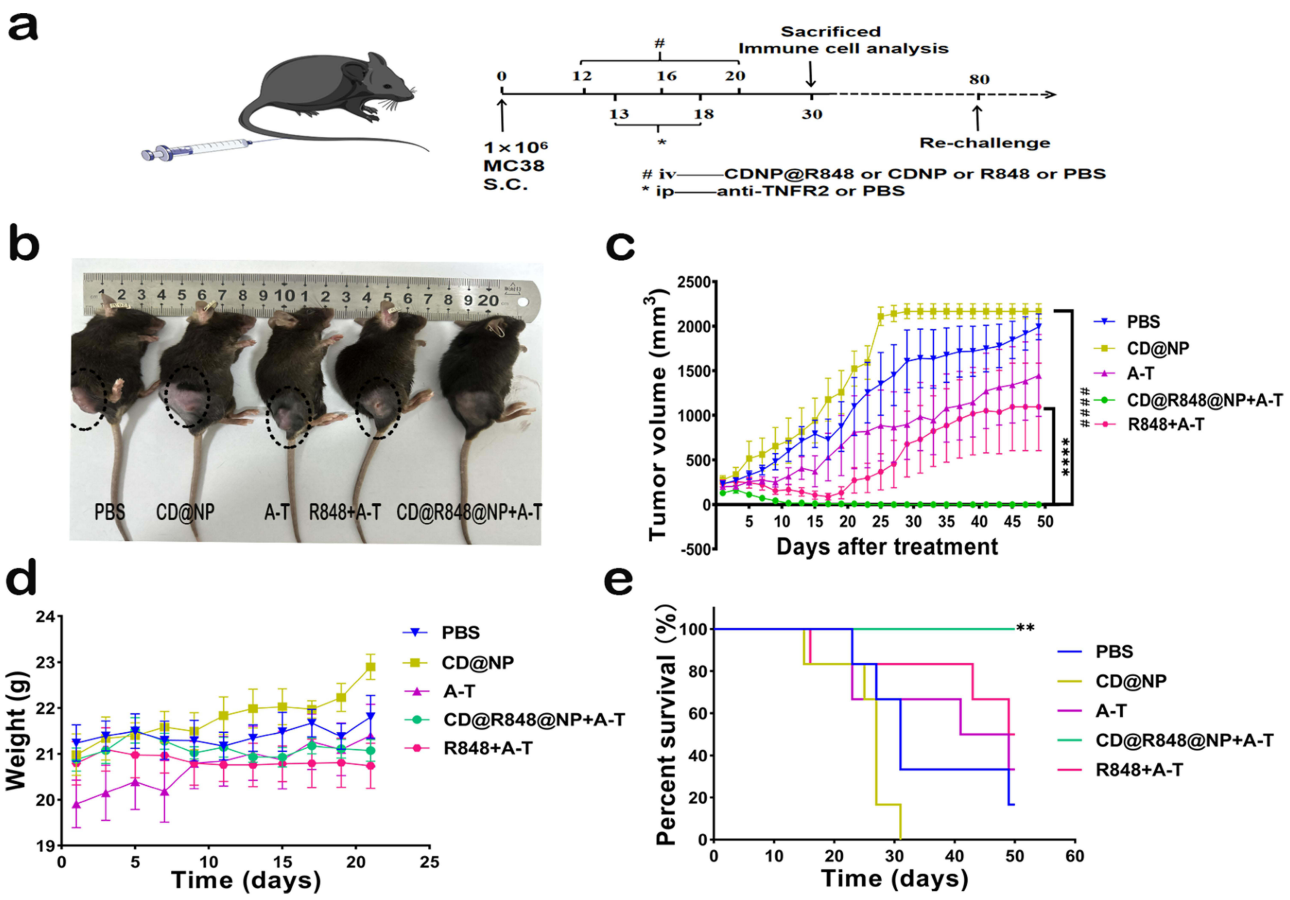

Figure 7 Antitumor effects on mice with colon cancer: (**a**) Construction of subcutaneous tumor model of C57BL/6J mice (6 weeks old) and schematic diagram of administration process. (**b**) Representative images of mice from each group were captured after the last dose (Day 38). Black dotted circles indicate MC38 tumor regions. (**c**) Tumor growth curve. n=6. The data are expressed as mean ± SEM and was analyzed with two-way ANOVA followed by Tukey's multiple comparisons test. ****P<0.0001 compared to R848+A-T; ####P<0.0001 compared to CD@NP; (**d**) Mouse body weight change curve. Body weight of mice in each group was monitored every two days. n = 6, data are expressed as mean ± SEM. (**e**) Survival curve of mice: comparison of the survival curves between each group. n=6; The Log rank test was employed for the analysis. Differences were considered significant at *p < 0.05, **p < 0.01, ***p < 0.001, and ****p <0.0001.

Notes: A-T: anti-TNFR2; R848: Resiquimod; NPs, bare PLGA nanoparticles; CD@NPs: PLGA nanocapsules modified with 2-HP-β-CD; CD@R848@NP: drug R848-loaded PLGA nanoparticles modified by 2-HP-β-CD; CD@R848@NP+A-T: CD@R848@NP+anti-TNFR2; R848+A-T: R848+anti-TNFR2.

To assess the biological safety of immune combination therapy, we performed euthanized and dissected the CD@R848@NPs+A-T group on day 10 after the last dose injection (Day 30). As shown in Supplementary Figure 3, staining of the main organs (heart, liver, spleen, lung, and kidney) revealed that the organs of the mice in the CD@R848@NP+A-T group were structurally intact, the cells were tightly arranged, and no noticeable lesions were observed. These results demonstrate the absence of toxic side effects and confirms the safety of the nanoparticle immune combination therapy.

Antitumor Immunity Activation of CD@R848@NPs in vivo

The combination of CD@R848@NPs and anti-TNFR2 (CD@R848@NPs+A-T) had a substantial anticancer effect on the MC38 CRC model. To elucidate the anticancer mechanism, the distribution of immune cells in the tumor, spleen and blood were analyzed via flow cytometry.

Compared with the other groups, the CD@R848@NPs+A-T group exhibited a reduced number of $CD4^+$ T cells and an increase in the number of $CD8^+$ T cells (Figure 8a–b) in spleen. Consistent with our observations in the spleen, the quantity of $CD8^+$ T cells was increased in the peripheral blood of the CD@R848@NPs+A-T group (Figure 8c–d).

As displayed in Figures 8e-f, there was an increase in the number of $F4/80^+$ CD11b macrophages and $F4/80^+$ CD11b $CD86^+$ cells in the CD@R848@NPs+A-T group. This finding suggested that CD@R848@NPs+A-T successfully polarized TAMs into antitumor macrophages.

As TAM polarization can increase the secretion of TNF-α, interleukin-12 (IL-12p70), and IL-6, an immunohistochemical staining assay was conducted to determine the cytokine concentration. The CD@R848@NP+A-T group exhibited considerably larger TNF-α and IL-6-positive regions than the other groups, as evidenced by the immunohistochemical images (Figure 8g).

The expression of CD206 (M2 polarization marker) in tumor tissues was determined by immunofluorescence staining. In contrast to those in the control group, tumors derived from the CD@R848@NPs+A-T group exhibited lower levels of CD206 expression (Figure 8h). This finding suggested that TAMs were successfully reprogrammed to function as M1-like antitumor effector cells.

To confirm that M2-like macrophage repolarization occurred, we collected blood and measured the secretion of IL-12, IL-6 and TNF-α using an enzyme-linked immunosorbent assay (ELISA). The results of the assay confirmed that higher levels of IL-12, IL-6, and TNF-α were secreted by macrophages subjected to CD@R848@NPs+A-T than by the control group (Figure 8i). These cytokines can promote innate and adaptive immune responses. CD@R848@NPs can deliver cytokines regionally to T cells in tumor tissues, enhancing the $CD8^+$ to regulatory T-cell ratio in tumor tissues and resulting in significantly improved antitumor efficacy against MC38 tumors.

Rechallenge Experiments in Tumor-Free Mice

To ascertain whether CD@R848@NP treatment elicited an "immune memory" response against MC38 tumors, CD@R848@NP+A-T group tumor-free mice were monitored 60 days after the last dose (Day 80). As Liver cancer and colon cancer are common primary solid tumors with high morbidity, and the liver is a common site of colon cancer metastasis. And the MC38 and Hepa1-6 cell lines are commonly used for liver and colon cancers, we selected these two cell lines for our study. Subsequently, the MC38 tumor cells were reintroduced into the rodents at the same site on the right side, whereas the Hepa1-6 cancer cells were introduced to the contralateral side. The findings revealed that the cured mice developed Hepa1-6 tumors but did not develop MC38 tumors (Figure 9a–b). This finding suggested that the treated mice developed tumor-specific immune memory.

Discussion

The objective of this study was to develop a novel nanoparticle system with high encapsulation efficiency to induce the transition of M2 macrophages to the M1 phenotype, and to enhance the immunotherapeutic efficacy of the system in mouse colon tumor models. To address issues of poor tumor penetration and low water solubility of conventional anticancer drugs, a nanodelivery system approach was utilized for combined immunotherapy. PLGA nanocarriers modified with 2-HP-β-CD

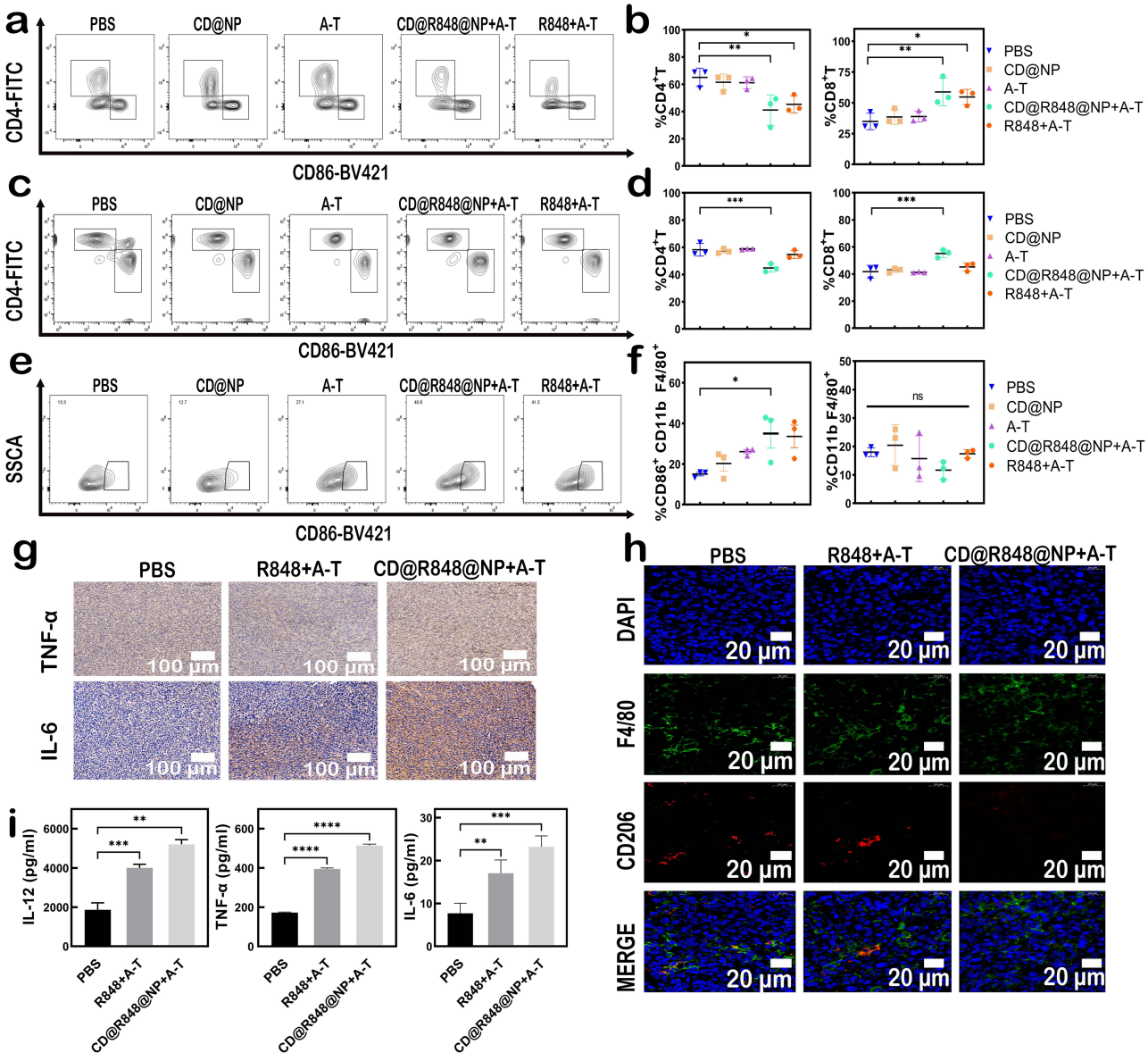

Figure 8 Evaluation of immune cell infiltration: (**a**) Representative dot plots of $CD4^+$ T cells among $CD8^+$ T cells in the spleens of mice. (**b**) Percentage of $CD4^+$ T cells among CD8+ T cells in the spleen. The results are presented as the mean ± SD. n =3. (**c**)Representative dot plots of $CD4^+$ T cells and $CD8^+$ T cells in the blood of mice. (**d**) Percentage of $CD4^+$ T cells and $CD8^+$ T cells in the blood. The results are presented as the mean ± SD. n =3. (**e**) TAM expression of CD86, a marker of M1-like macrophages. Representative flow cytometric plot of $CD86^+$ cells among $CD11b^+$ $F4/80^+$ cells. (**f**) Percentage of $CD11b^+$ $F4/80^+$ $CD86^+$ and $CD11b^+$ $F4/80^+$ cells in the tumor tissues. Data are expressed as mean ± SEM. n =3. (**g**) Immunohistochemical staining for the tumor tissue, TNF-α, and IL-6 staining images of the tumor tissues. Scale bar: 100 μm. (**h**) Immunofluorescence staining of CD206 cells (red) in the tumor tissues. Scale bar: 20 μm. (**i**) TNF-α, IL-6, and IL-12 levels of plasma were tested by ELISA. Differences were considered significant at *p < 0.05, **p < 0.01, ***p < 0.001, and ****p <0.0001 according to one-way analysis of variance (ANOVA) (b, d, and f).

were employed to encapsulate R848 (CD@R848@NPs), enhancing water solubility and leveraging affinity for macrophages to modulate the tumor microenvironment. In vitro, CD@R848@NPs demonstrated high biocompatibility and released over 70% of the drug in acidic conditions (Figure 3). Nanoparticles modified with 2-HP-β-CD (CD@R848@NP) exhibited superior tumor localization and effectively induced M1 macrophage polarization, upregulating expression of key genes (Cd80, TNF-α, Nos2) (Figure 5). In vivo, CD@R848@NP combined with anti-TNFR2 successfully eradicated subcutaneous colon cancer tumors and regulate the infiltration of $CD8^+$T cells, the mice showed increased levels of IL-12, TNF-α and IL-6 in the plasma (Figure 8i). Notably, free R848 treatment combined with anti-TNFR2 inhibited the growth of tumors at an early stage but promoted immune tolerance and tumor hyperprogression in vivo, indicating that CD@R848@NPs+A-T achieved a better therapeutic effect.

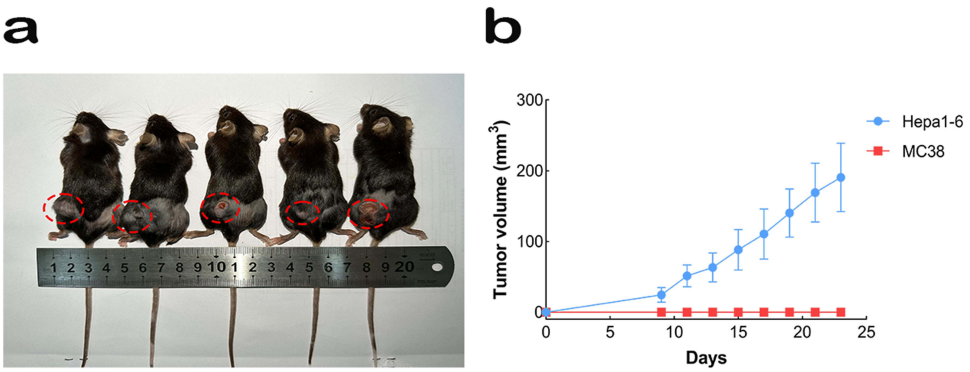

Figure 9 Rechallenge assay in tumor-free mice: (**a**) Tumor growth maps of tumor rechallenged mice. Red dotted circles indicate Hepa1-6 tumor regions. The results were repeated three times, and similar results were obtained (n = 5). (**b**) To generate tumor growth curves, 2×10^5 cells/mL MC38 cells were subcutaneously injected into tumor-free mice, while an equal number of Hepa1-6 cells were injected into the left side. The red line in the curve corresponds to MC38 cells, while the blue line represents Hepa1-6 cells. The results are presented as the means ± SEMs.

Cancer thrives in an environment that suppresses the immune system. The effectiveness of immunotherapy is influenced by the immunosuppressive microenvironment of the tumor, which is primarily caused by M2 macrophages.[32] Immunosuppressive cells prevalent in the tumor microenvironment primarily include TAMs, MDSCs, and Tregs.[33] TAMs exhibit a high degree of adaptability with opposing phenotypes and functions, which can either support tumor growth (eg, M2-like cells) or exhibit tumor-killing abilities (eg, M1-like cells).[34] Han et al developed a PLGA nanodrug delivery system loaded with M2 macrophage-binding peptides that target M2, facilitating the specific transportation of baicalin, tumor antigens, and immune stimulators and augmenting antitumor immune responses.[35] This study focused on cyclodextrins (CDs), a group of macrocyclic oligosaccharides connected by α-1,4 glycosidic bonds. The CDs consisted of α-, β-, and γ-CDs, which contained 6, 7, and 8 glucose units, respectively. Specifically, 2-HP-β-CD was formed by substituting the second hydroxyl group in the β-CD structure with a hydroxypropyl group.[36] In contrast to CDs, β-CDs have demonstrated exceptional biocompatibility, distinct inclusion capacities, and potent functionalization capacities. Due to these attributes, CDs and their derivatives are appealing options for developing innovative functional materials for biomedical applications.[37]

Consequently, PLGA was modified using β-CD to serve as a delivery vehicle for tumor immunotherapy. One of the main goals of cancer research is to develop novel therapies that can successfully slow the growth of tumors and prevent side effects, such as cachexia. Combination immunotherapy is a novel approach in this field. Anfray et al demonstrated that the poly(I:C) +R848 combination was more effective than any individual intervention, including R837.[38] Additionally, researchers have discovered that compared to immunotherapy, targeted therapy is rapid and brief; thus, the two treatments might be combined to enhance one another's advantages. When used in conjunction with CDNPs, PD-1 antibodies can effectively reduce the growth of B16 tumors.[23] Our preliminary studies demonstrated that combining HMGN1 and 3M-052 with an anti-TNFR2-stimulated DC vaccine can effectively enhance the activation of CTLs by targeting Treg cells and immature DCs.[39] This dual-targeted immunosuppression approach results in homologous immune memory and effective antitumor effects.[39] As a result, we employed an immunotherapy combination along with a nanodelivery method, and the outcomes met our expectations. Our study has certain limitations. For instance, other studies have indicated that active targeted nanomedicine delivery systems are superior to passive EPR methods.[40] Although more research is needed to determine the exact mechanism involved, some experts speculate that the mechanism involves the attraction of the dextran structure to macrophages.[41] Consequently, enhancing the capacity of drug-targeted delivery in conjunction with immunological and oncological advancements would contribute to the development of safer and more efficient tumor immunotherapies.

Conclusion

To achieve tumor clearance in colon cancer model, the current study proposed a novel immunotherapy strategy using a nanodelivery method. This strategy utilizes the inherent affinity of 2-HP-β-CD for macrophages, enabling the targeted and efficient delivery of TLR agonist (R848) to TIME and reprogramming tumor-promoting M2-like macrophages toward a M1 phenotype with reduced systemic side effects in a specific manner. And in vitro experiments revealed that the

nanoparticles were non-toxic, biocompatible and exhibited excellent macrophage targeting. Furthermore, CD@R848@NP combined with anti-TNFR2 results in remarkable activation of antitumor effects and even confer antitumor immune memory, demonstrated as resistance to tumor rechallenge in treated mice. This study demonstrated the nanodelivery systems are important in tumor-targeting therapy which providing a valuable tool to improve outcomes in patients with solid tumors including colon cancer. These nanomaterials can also be used to encapsulate different hydrophobic medications, providing a versatile platform for the treatment of various diseases.

Abbreviations

PLGA, poly (lactic-co-glycolic acid); CRC, Colorectal cancer; TEM, Transmission Electron Microscope; TLR, Toll-like receptor; TAM, tumor-associated macrophage; TIME, tumor immune microenvironment; Tregs, $CD4^{+}Foxp3^{+}$ regulatory T cells; A-T, anti-TNFR2; CD, β-cyclodextrin; R848, Resiquimod; NPs, bare PLGA nanoparticles; CD@NPs, PLGA nanocapsules modified with 2-HP-β-CD; R848@NPs, R848 coated with PLGA nanoparticles; CD@R848@NP, drug R848-loaded PLGA nanoparticles modified by 2-HP-β-CD; CD@R848@NP+A-T, CD@R848@NP+anti-TNFR2; R848+A-T, R848+anti-TNFR2; IR-780-R848@NPs, the drug R848 and IR-780 dye loaded with PLGA nanoparticles; IR-780-CD @R848@NPs, the drug R848 and IR-780 dye loaded with PLGA nanoparticles modified with 2-HP-β-CD.

Ethics Approval

All animal-related procedures were carried out based on an approved protocol from the institutional animal care and treatment committee (license number for laboratory animals: EAE-GZU-2022-7088). Protocol for animals study were approved by Institutional Animal Care Committee of Guizhou University.

Author Contributions

All authors made a significant contribution to the work reported, whether that is in the conception, study design, execution, acquisition of data, analysis, and interpretation, or in all these areas; took part in drafting, revising, or critically reviewing the article; gave final approval of the version to be published; have agreed on the journal to which the article has been submitted; and agree to be accountable for all aspects of the work.

Funding

This work was supported by the National Natural Science Foundation of China (82060308) and, National Key Laboratory of Respiratory. Diseases (SKLRD-OP-202208), Guizhou Provincial Science and Technology Projects (GPPH-NSFC-2020-6; GPPH-NSFC-2020-7; GCC [2022]037-1), Guizhou Provincial Basic Research Program (Natural Science) (No. Qiankehe-Basic-ZK[2021]-general 405, Qiankehe-Basic-ZK [2021]-general-556), Qiankehe-basic-ZK-[2024]-general-072), Health Commission of Guizhou Province (Grant Number: gzwkj2022-004), the 2018 Talent Research Program of Guizhou University (2018-53), Guizhou University Talent Introduction Research Project (No. Guidarenjihezi (2020) number 76) and the funding from Ministry of Human Resources and Social Security of the People's Republic of China.

Disclosure

The authors report no conflicts of interest in this work.

References

1. Sung H, Ferlay J, Siegel RL. et al. Global cancer statistics 2020: GLOBOCAN estimates of incidence and mortality worldwide for 36 cancers in 185 Countries. *CA*. 2021;71(3):209–249. doi:10.3322/caac.21660
2. Arbyn M, Weiderpass E, Bruni L, et al. Estimates of incidence and mortality of cervical cancer in 2018: a worldwide analysis. *Lancet Glob Health*. 2020;8(2):e191–e203. doi:10.1016/S2214-109X(19)30482-6
3. Dai Z, Yu X, Hong J, Liu X, Sun J, Sun X. Development of a novel CsA-PLGA drug delivery system based on a glaucoma drainage device for the prevention of postoperative fibrosis. *Mater Sci Eng C*. 2016;66:206–214. doi:10.1016/j.msec.2016.04.077
4. Vanamee ÉS, Faustman DL. TNFR2: a novel target for cancer immunotherapy. *Trends Mol Med*. 2017;23(11):1037–1046. doi:10.1016/j.molmed.2017.09.007

5. Binnewies M, Roberts EW, Kersten K, et al. Understanding the tumor immune microenvironment (TIME) for effective therapy. *Nature Med*. 2018;24(5):541–550. doi:10.1038/s41591-018-0014-x
6. Shamdani S, Uzan G, Naserian S. TNFα-TNFR2 signaling pathway in control of the neural stem/progenitor cell immunosuppressive effect: different experimental approaches to assess this hypothetical mechanism behind their immunological function. *Stem Cell Res Ther*. 2020;11(1):307. doi:10.1186/s13287-020-01816-2
7. Da Silva CG, Camps MGM, Tmwy L, et al. Effective chemoimmunotherapy by co-delivery of doxorubicin and immune adjuvants in biodegradable nanoparticles. *Theranostics*. 2019;9(22):6485–6500. doi:10.7150/thno.34429
8. Cassetta L, Pollard JW. Targeting macrophages: therapeutic approaches in cancer. *Nat Rev Drug Discov*. 2018;17(12):887–904. doi:10.1038/nrd.2018.169
9. Pan Y, Yu Y, Wang X, Zhang T. Tumor-associated macrophages in tumor immunity. *Front Immunol*. 2020;11:583084. doi:10.3389/fimmu.2020.583084
10. Rong L, Zhang Y, Li W-S, Su Z, Fadhil JI, Zhang C. Iron chelated melanin-like nanoparticles for tumor-associated macrophage repolarization and cancer therapy. *Biomaterials*. 2019;225:119515. doi:10.1016/j.biomaterials.2019.119515
11. Deng R-H, Zou M-Z, Zheng D, et al. Nanoparticles from cuttlefish ink inhibit tumor growth by synergizing immunotherapy and photothermal therapy. *ACS nano*. 2019;13(8):8618–8629. doi:10.1021/acsnano.9b02993
12. Jiang M, Liu J, Yang D, et al. A TNFR2 antibody by countering immunosuppression cooperates with HMGN1 and R848 immune stimulants to inhibit murine colon cancer. *Int Immunopharmacol*. 2021 101;108345 doi:10.1016/j.intimp.2021.108345
13. Smith M, García-Martínez E, Pitter MR, et al. Trial watch: toll-like receptor agonists in cancer immunotherapy. *OncoImmunology*. 2018;7(12):e1526250. doi:10.1080/2162402X.2018.1526250
14. Dietsch GN, Lu H, Yang Y, et al. Coordinated activation of toll-like receptor8 (TLR8) and NLRP3 by the TLR8 agonist, VTX-2337, ignites tumoricidal natural killer cell activity. *PLoS One*. 2016;11(2):e0148764. doi:10.1371/journal.pone.0148764
15. Rook AH, Gelfand JM, Wysocka M, et al. Topical resiquimod can induce disease regression, eradicate malignant T cells and enhance T cell effector functions in cutaneous T cell lymphoma. Blood. 2015. doi:10.1182/blood-2015-02-630335
16. Engel AL, Holt GE, Lu H. The pharmacokinetics of Toll-like receptor agonists and the impact on the immune system. *Expert Rev Clin Pharmacol*. 2011;4(2):275–289. doi:10.1586/ecp.11.5
17. Varshney D, Qiu SY, Graf TP, McHugh KJ. Employing drug delivery strategies to overcome challenges using TLR7/8 agonists for cancer immunotherapy. *AAPS J*. 2021;23(4):90. doi:10.1208/s12248-021-00620-x
18. Lan H, Zhang W, Jin K, Liu Y, Wang Z. Modulating barriers of tumor microenvironment through nanocarrier systems for improved cancer immunotherapy: a review of current status and future perspective. *Drug Delivery*. 2020;27(1):1248–1262. doi:10.1080/10717544.2020.1809559
19. Qodratnama R, Serino LP, Cox HC, Qutachi O, White LJ. Formulations for modulation of protein release from large-size PLGA microparticles for tissue engineering. *Mater Sci Eng C*. 2015;47:230–236. doi:10.1016/j.msec.2014.11.003
20. Makadia HK, Siegel SJ. Poly Lactic-co-Glycolic Acid (PLGA) as biodegradable controlled drug delivery carrier. *Polymers*. 2011;3(3):1377–1397. doi:10.3390/polym3031377
21. Santos AC, Costa D, Ferreira L, et al. Cyclodextrin-based delivery systems for in vivo-tested anticancer therapies. *Drug Delivery Transl Res*. 2021;11(1):49–71. doi:10.1007/s13346-020-00778-5
22. Zheng K, Huang Z, Huang J, et al. Effect of a 2-HP-β-cyclodextrin formulation on the biological transport and delivery of chemotherapeutic PLGA nanoparticles. *Drug Des Devel Ther*. 2021;15:2605–2618. doi:10.2147/DDDT.S314361
23. Rodell CB, Arlauckas SP, Cuccarese MF, et al. TLR7/8-agonist-loaded nanoparticles promote the polarization of tumour-associated macrophages to enhance cancer immunotherapy. *Nat Biomed Eng*. 2018;2(8):578–588. doi:10.1038/s41551-018-0236-8
24. Ren B, Jiang B, Hu R, et al. HP-β-cyclodextrin as an inhibitor of amyloid-β aggregation and toxicity. *Phys Chem Chem Phys*. 2016;18(30):20476–20485. doi:10.1039/C6CP03582E
25. Facciabene A, Motz GT, Coukos G. T-regulatory cells: key players in tumor immune escape and angiogenesis. *Cancer Res*. 2012;72(9):2162–2171. doi:10.1158/0008-5472.CAN-11-3687
26. Fonseca C, Simões S, Gaspar R. Paclitaxel-loaded PLGA nanoparticles: preparation, physicochemical characterization and in vitro anti-tumoral activity. *J Control Release*. 2002;83(2):273–286. doi:10.1016/S0168-3659(02)00212-2
27. Perveen K, Husain FM, Qais FA, et al. Microwave-assisted rapid green synthesis of gold nanoparticles using seed extract of trachyspermum ammi: ROS mediated biofilm inhibition and anticancer activity. *Biomolecules*. 2021;11(2):197. doi:10.3390/biom11020197
28. Mazumder S, Dewangan AK, Pavurala N. Enhanced dissolution of poorly soluble antiviral drugs from nanoparticles of cellulose acetate based solid dispersion matrices. *Asian J. Pharm. Sci.* 2017;12(6):532–541. doi:10.1016/j.ajps.2017.07.002
29. Gong X, Zheng Y, He G, Chen K, Zeng X, Chen Z. Multifunctional nanoplatform based on star-shaped copolymer for liver cancer targeting therapy. *Drug Deliv*. 2019;26(1):595–603. doi:10.1080/10717544.2019.1625467
30. Yao J, Li Y, Sun X, Dahmani FZ, Liu H, Zhou J. Nanoparticle delivery and combination therapy of gambogic acid and all-trans retinoic acid. *Int J Nanomed*. 2014;9:3313–3324. doi:10.2147/IJN.S62793
31. Ding W, Guo L. Immobilized transferrin Fe3O4@SiO2 nanoparticle with high doxorubicin loading for dual-targeted tumor drug delivery. *Int J Nanomed*. 2013;8:4631–4639. doi:10.2147/IJN.S51745
32. Xie X, Li S, Liu Y, et al. Based on functional materials and PLGA for the florfenicol controlled release system and its antibacterial properties. *React Funct Polym*. 2022;178:105331. doi:10.1016/j.reactfunctpolym.2022.105331
33. Pitt JM, Marabelle A, Eggermont A, Soria JC, Kroemer G, Zitvogel L. Targeting the tumor microenvironment: removing obstruction to anticancer immune responses and immunotherapy. *Ann Oncol*. 2016;27(8):1482–1492. doi:10.1093/annonc/mdw168
34. Wang NX, von Recum HA. Affinity-based drug delivery. *Macromol biosci*. 2011;11(3):321–332. doi:10.1002/mabi.201000206
35. Han S, Wang W, Wang S, et al. Tumor microenvironment remodeling and tumor therapy based on M2-like tumor associated macrophage-targeting nano-complexes. *Theranostics*. 2021;11(6):2892–2916. doi:10.7150/thno.50928
36. Hayashi T, Crain B, Corr M, et al. Intravesical Toll-like receptor 7 agonist R-837: optimization of its formulation in an orthotopic mouse model of bladder cancer. *International Journal of Urology: Official Journal of the Japanese Urological Association*. 2010;17(5):483–490. doi:10.1111/j.1442-2042.2010.02503.x
37. Lipkowitz KB. Applications of Computational Chemistry to the Study of Cyclodextrins. *Chem Rev*. 1998;98(5):1829–1874. doi:10.1021/cr9700179

38. Anfray C, Mainini F, Digifico E, et al. Intratumoral combination therapy with poly(I:C) and resiquimod synergistically triggers tumor-associated macrophages for effective systemic antitumoral immunity. *Journal for ImmunoTherapy of Cancer*. 2021;9(9):e002408. doi:10.1136/jitc-2021-002408
39. Zhu L, Zhang X, Chen X, et al. Anti-TNFR2 enhanced the antitumor activity of a new HMGN1/3M-052 stimulated dendritic cell vaccine in a mouse model of colon cancer. *Biochem Biophys Res Commun* 2023;653:106–114. doi:10.1016/j.bbrc.2023.02.039
40. Combes F, Meyer E, Sanders NN. Immune cells as tumor drug delivery vehicles. *J Control Release*. 2020;327:70–87. doi:10.1016/j.jconrel.2020.07.043
41. Pandit S, Dutta D, Nie S. Active transcytosis and new opportunities for cancer nanomedicine. *Nature Mater*. 2020;19(5):478–480. doi:10.1038/s41563-020-0672-1